Cement and Concrete Composites 73 (2016) 54–61

Contents lists available at ScienceDirect

Cement and Concrete Composites

journal homepage: www.elsevier.com/locate/cemconcomp

Dielectric characterization of concrete at high temperatures

Sergey Soldatov [a, *], Martin Umminger [b], Annette Heinzel [a], Guido Link [a], Benjamin Lepers [a], John Jelonnek [a, c]

[a] Karlsruhe Institute of Technology (KIT), Institute for Pulsed Power and Microwave Technology (IHM), Hermann-von-Helmholtz-Platz 1, 76344, Eggenstein-Leopoldshafen, Karlsruhe, Germany
[b] Karlsruhe Institute of Technology (KIT), Institute of Concrete Structures and Building Materials (IMB), Gotthard-Franz-Straße 3, 76131, Karlsruhe, Germany
[c] Karlsruhe Institute of Technology (KIT), Institute of Microwaves and Electronics (IHE), Kaiserstraße 12, 76131, Karlsruhe, Germany

ARTICLE INFO

Article history:
Received 8 June 2015
Received in revised form
26 January 2016
Accepted 30 January 2016
Available online 23 June 2016

Keywords:
Complex permittivity
Electric properties
Microwave processing
High temperature
Portland cement concrete
Thermogravimetry

ABSTRACT

For reliable modelling of microwave heating of concrete its complex permittivity has to be known precisely within the full range of working temperatures. Dielectric characterization of dry concrete cured with different water-to-cement (w/c) ratios and concrete samples from nuclear power plant constructions was performed during heating and cooling cycles from room temperature to 700 °C and back. On average, higher permittivity values are found for concretes cured with smaller w/c ratio (more dens and less porous) as compared to concretes cured with higher w/c ratio (lighter and more porous). Samples from nuclear power plant reveals a permittivity close to the concrete prepared with lowest w/c ratio. Permittivity change along increasing temperature correlates with moisture loss and thermal decomposition reactions. These reactions are irreversible that lead to a permittivity divergence in heating and cooling scenarios. The variations of concrete permittivity because of w/c ratio, water transport and decomposition reactions are discussed.

1. Introduction and motivation

After water, concrete is the second most consumed product on Earth [1]. Because of its broad usage in industry works and civil engineering its processing and utilization are urgent issues. Traditionally, for demolition and dismantling of concrete structures, mechanical electric rotary or pneumatic tools are used. Besides pneumatic breakers, also hydraulic and ultrasonic breakers are sometimes used. All the above methods, however, have significant health hazards because of generation of high level of noise, dust and/or vibrations.

In recent decades, microwave technologies are progressively replacing traditional heating and processing techniques. Similarly, in the concrete industry, the application of microwave has shown a high potential for applications, such as a selective demolition and drilling of concrete [2]. Such advantages as contactless and low noise processing, time and energy saving, sufficient reduction of dust and debris, and much less cross-contamination (when used for surface deactivation of radioactive concrete) make it attractive for industry. The first patents for breaking of rocks [3] and demolition of concrete with microwaves [4,5] in the end of 1960s were followed by research activities in Japan (JAERI), UK (Harwell Laboratory) and USA (ORNL) [6,7] on the methods and necessary equipment for microwave demolition of concrete. Later, the development of sophisticated, non-destructive methods for investigation of micro-structure of concrete (see e.g. Ref. [8]) as well as the progress in theory and numerical simulations of microwave heating of concrete (see Refs. [9–12]) have advanced the understanding of the mechanisms of the breakage and durability of concrete.

For calculation of thermal stresses and strains which lead to breakage of concrete, the absorbed microwave power P_{abs} has to be known. It is directly proportional to the relative dielectric loss factor ε_r'' of the material and reads as follows: $P_{abs} = 2\pi f \varepsilon_0 \varepsilon_r'' E_{rms}^2$. Here f, ε_0 and E_{rms} are the frequency, dielectric constant of vacuum

* Corresponding author. Karlsruhe Institute of Technology (KIT), Institute for Pulsed Power and Microwave Technology (IHM), Hermann-von-Helmholtz-Platz 1, Bldg. 421, 76344, Eggenstein-Leopoldshafen, Germany.
E-mail addresses: sergey.soldatov@kit.edu (S. Soldatov), martin.umminger@kit.edu (M. Umminger), annette.heinzel@kit.edu (A. Heinzel), guido.link@kit.edu (G. Link), benjamin.lepers@kit.edu (B. Lepers), john.jelonnek@kit.edu (J. Jelonnek).

http://dx.doi.org/10.1016/j.cemconcomp.2016.01.006
0958-9465/

and the root mean square amplitude of the electric field in the material, respectively. The latter one also depends on the reflection from a concrete surface that is influenced by the real part of the relative permittivity of concrete ε_r'. Therefore, for process modelling and reliable design of a microwave applicator the complex permittivity ($\varepsilon_r = \varepsilon_r' - j{\cdot}\varepsilon_r''$) has to be known precisely and *within a full range of the working temperatures*. The necessity of temperature dependent permittivity data for correct modelling of microwave demolition of concrete was recognized in the work of W. Li et al. where the power dissipation and temperature distribution profiles were modelled for four frequencies: 0.896, 2.45, 10.6 and 18.0 GHz [10]. Also in their work, W. Li and coauthors have performed the temperature dependent measurements of concrete dielectric properties within 20 … 250 °C with a step of 50 °C and with the use of the coaxial probe method.

In subsequent years several measurements of permittivity of concrete, though performed at ambient temperature, were reported. At different moisture conditions (wet, saturated, air dried and oven dried) and frequencies within 0.1 … 20 GHz the permittivity of concrete was reported in Ref. [13]. Dielectric properties of concrete, both with and without composites, with different w/c ratios and within 0–1 GHz are published in Ref. [14] where a transmission line method is used. A Portland cement concrete prepared with different w/c ratios was characterized at frequencies from 0.1 to 1 GHz with the use of the coaxial transmission line method in Ref. [15]. With the measurement of the time delay in an "open space method" the evaluation of dielectric properties of a Portland cement concrete with w/c = 0.6 and within 8 … 18 GHz was performed in Ref. [16]. Noteworthy, all abovementioned experiments were performed at room temperature. To our knowledge, the permittivity of concrete exposed to elevated temperatures up to 700 °C and thereafter cooled back to room temperature has not been investigated yet in the literature.

In this work we investigate both, concrete cured in the lab with different w/c ratios as well as samples cut from concrete constructions of a real nuclear power plant. Such particular interest in nuclear power plant concrete is stimulated by the microwave ablation technique proposed for the removal of the upper (most radioactively contaminated) layer of the massive concrete blocks of the reactor compartment as a promising tool for its decontamination after decommissioning [5,6]. For abovementioned types of concrete the complex permittivity has been measured experimentally at the microwave frequency of 2.45 GHz during heating cycles starting from room temperature up to 700 °C and during subsequent cooling back to room temperature. The experimental setup and the description of grades of concrete are presented in sections 2 and 3, respectively. Experimental results for permittivity measurements and thermogravimetric analysis are given in section 4, and discussed in section 5. The conclusions are outlined in section 6.

2. Setup for dielectric measurements

For permittivity measurements a system based on the cavity perturbation method is used (see Fig. 1). The cavity perturbation method inherently is more precise than coaxial probe or reflection/transmission methods. The rectangular cavity is operated at the fundamental $TE_{1,0,4}$–mode and a resonance frequency close to 2.45 GHz. The transmission factor S_{21} is measured with a vector network analyzer (VNA) connected to the input and output port of the cavity. The temperature of the sample is controlled with an infrared pyrometer, looking to the sample surface through a small aperture in the cavity's wall. The maximum transmission coefficient at resonance and without perturbation is −36 dB and the Q-factor is about 12000. The sample is heated inside a conventional tubular furnace placed nearby the cavity. For every predefined temperature the sample first is heated in the furnace and thereafter moved to the measurement position in the cavity. To reduce the sample cooling when it moves from the oven into the cavity and to decrease heat transfer from heater to cavity, an insulating block is mounted between the furnace and the resonator. For sample positioning inside the cavity a quartz tube with an outer diameter of 10 mm and an inner diameter of 8 mm is used as a sample holder. Additionally, the quartz tube serves as a thermal insulator and a heat container preventing too fast cooling of the sample and reducing temperature gradients in the sample. The heating and positioning of the sample as well as the data acquisition are fully automatized using a personal computer. A more detailed description of the apparatus can be found in Ref. [17]. In our experiments we used cylindrical concrete samples with about 8 mm in diameter and 10 mm in height (~0.5 cm^3 in volume).

3. Grades of concrete

In the present work we investigate concrete samples taken from a real nuclear power plant construction as well as samples prepared on place. The blocks of concrete type BK28 were cut from the concrete construction of the nuclear power plant in Zwentendorf, Austria. The reactor built in 1972 was never put into operation and therefore its constructions and buildings are absolutely free from radioactive contamination. Nowadays it is used as a museum, for teaching of students and for scientific research purposes. The interest in concrete from nuclear power plants was stimulated by the microwave ablation technique used for the removal of upper layers of the massive concrete blocks of the reactor for its decontamination [5,6]. The samples for the present investigation were cut from concrete walls of the machinery hall of the nuclear power plant.

The concrete materials assigned as M1, M2 and M3 were prepared by the Institute of Concrete Structures and Building Materials (IMB). Their main properties are summarized in Table 1 and detailed characteristics can be found in Ref. [18]. The samples M1–M3 were made with different w/c ratios and therefore differ in density and porosity. The amount of water used for cement paste preparation influences the final porosity of concrete. This is because the space occupied by the admixed water is converted into porosity as a result of cement hydration and an evaporation of residual water into the environment. Therefore the higher the w/c ratio, the larger the pore volume or porosity (see Table 1). The relative volumes of aggregates and cement paste for M1—M3 grades were kept the same, 70% and 30% respectively.

The aggregates used in M1–M3 mixtures are listed in Table 2. Note, that calcareous aggregates such as limestone and the sandstone with carbonate group become unstable at $T > 500$ °C and dissociate into calcium oxide and CO_2 [19]. All residual aggregates are usually stable at least up to 800 °C [19]. All aggregates used in M1–M3 mixtures have relatively high hydraulic permeability as compared to cement paste. Typical permeability of granite and sandstone are about $5{\cdot}10^{-9}$ cm/s and $12{\cdot}10^{-9}$ cm/s, respectively [20]. For comparison, the cement paste permeability is about $6{\cdot}10^{-11}$ cm/s [20].

To compare the composition of different concretes, the energy dispersive X-ray (EDX) analysis is utilized for all concretes under investigation. The results are summarized in Table 3. Note, for M1–M3 grades the concentration of main elements such as O, Si and Ca are very close. The much higher calcium concentration in BK28 (19.26%) indicates the higher percentage of calcareous aggregates (limestone) used in this concrete mix. To a less extent this difference may be referred to the difference in cement pastes where a portlandite $Ca(OH)_2$ is the main component. At the same time the depletion of silicon (17.99%) in BK28 concrete, as compared with

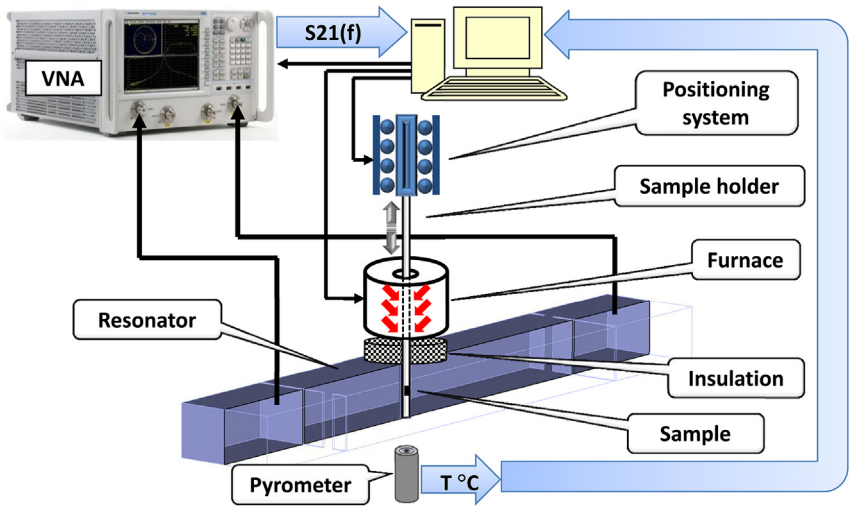

Fig. 1. Scheme of the system for dielectric measurements.

Table 1
Properties of different grades of concrete.

Concrete grade	Cement mortar [Vol %]	aggregates [Vol %]	dry density [g/cm^3]	W/c ratio [–]	Porosity [%]
M1	30	70	2.30	0.40	13.34
M2	30	70	2.26	0.55	15.06
M3	30	70	2.21	0.70	17.28
BK28			2.34		11.48

Table 2
Aggregates used for concretes M1—M3 production.

Aggregates	[Weight %]
Sandstone	36.6
Granite	23.0
Limestone	18.2
Quartzite	14.9
Sandstone with carbonate group	7.0
Gneiss	0.3

Table 3
EDX Measurement of concrete [weight %].

	M1	M2	M3	BK28
O	55.52	57.82	56.21	57.98
Na	1.57	0.07	0.32	0.23
Mg	0.40	0.20	0.26	1.45
Al	5.21	1.33	3.14	1.50
Si	26.76	30.67	27.09	17.99
K	2.47	0.53	2.35	0.91
Ca	6.70	8.39	9.56	19.26
Fe	1.37	1.00	1.09	0.68

The lines for Si and Ca are highlighted because they indicate the difference in the aggregation (calcareous against siliceous) of concretes M1–M3 and BK28.

others concretes, reveals a reduced content of siliceous aggregates.

4. Experimental results

4.1. Thermogravimetric analysis

The microwave radiation being absorbed in concrete results in volumetric heating. At elevated temperature the dehydration of concrete starts. However, water evaporation is not the only reaction occurring in the concrete exposed to microwave heating. Several other reactions accompanied by the mass loss may take place [21]. To understand this dynamics a thermogravimetric analysis was employed. Thermogravimetry (TG) is a standard analysis that shows the change of mass of the sample as a function of temperature. For small pieces of concrete a TG analysis was performed for a temperature range from room temperature (RT) up to 750 °C with a heating rate of 3.5 °C/min.

Because of the restriction of the TG device on the maximal mass variation, the samples are limited to volumes smaller than 70 mm^3. The samples are manually selected in such way that the samples represent both aggregates and cement paste best. Because of that the volume ratio of cement mortar and aggregates for selected

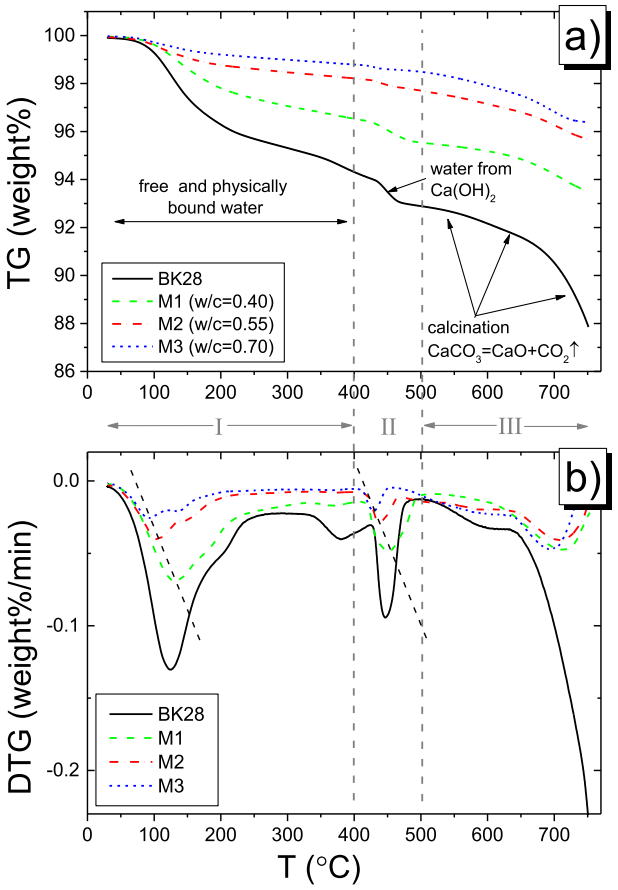

Fig. 2. Thermogravimetric analysis. (a) Mass loss (TG) and (b) differential mass loss (DTG) for four grades of concrete. Labels I, II and III and grey vertical dashed lines indicate temperature regions. Black dashed lines guide the shift of maximal mass loss rates in regions I and II.

samples may some differ from those indicated in Table 1. In Fig. 2 both TG and the time derivative of mass loss (DTG) are presented. Taking into account the results obtained we distinguish the following three temperature regions where three prevalent reactions take place: i) RT < T < 400 °C; ii) 400 °C < T < 500 °C; iii) 500 °C < T < 750 °C.

4.1.1. Mass loss at elevated temperature from RT to 400 °C (region I)

Within RT < T < 400 °C (region I) the dominating process is the evaporation of free and physically bound water [19]. This region may be almost completely referred to the water content in concrete (theoretically no free water exists for T > 374 °C [21]). Considering T = 350 °C as "no water point" we can estimate the dynamics of moisture concentration in concretes under investigation. It is presented in Fig. 3. The highest initial water concentration, ~5.0% is recorded for BK28. For M1, M2 and M3 water content is 3.2%, 1.6% and 1.1% respectively (see Fig. 3). From DTG data we can see that besides the difference in water content the rate of evaporation is also different. It is maximal for BK28 and decreases from type M1 to M3. Remarkably, for different concrete grades the maximal rate of water evaporation is reached at different temperatures. For BK28 and M1 it is at ~115 °C, for M2 at ~105 °C and for M3 at ~95 °C (this shift of maximum is guided in Fig. 2b with a dashed black line). The difference may be attributed to the difference in hydraulic permeability resulting from the difference in pore size distribution for M1—M3 concrete grades [18].

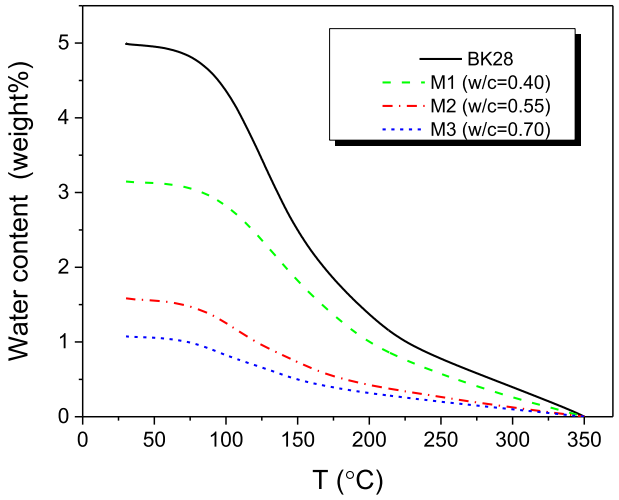

Fig. 3. Water content along increasing temperature. No water is assumed for T > 350 °C.

4.1.2. Mass loss at elevated temperature from 400 to 500 °C (region II)

Within 400 < T < 500 °C (region II) chemically bound water releases because of the thermal decomposition of portlandite [19]: $Ca(OH)_2 \rightarrow CaO + H_2O$. Because of high temperature the released water evaporates much more intensively as compared to evaporation of free water in temperature region I and results in narrower peaks in the DTG plot (see Fig. 2b). For M1, M2 and M3 grades the amount of released water reduces gradually in accordance with their w/c ratios. The shift of the DTG maximum for different samples (also guided in Fig. 2b with dashed line) is about of the same order as for the peak in region I. It again indicates the difference in water transport related to the different pores structure in the concretes under investigation.

4.1.3. Mass loss at elevated temperature from 500 to 750 °C (region III)

Within 500 … 750 °C (region III) a calcium carbonate, mostly present in aggregates, decomposes (calcination): $CaCO_3 \rightarrow CaO + CO_2\uparrow$ [19]. The weight loss rates for M1, M2 and M3 are very close to each other and reach the maximum at ~700 °C (see region III in Fig. 2 b). It agrees well with the fact that for these mixes the same aggregate composition and percentage are used. As for BK28, its weight loss rate shows different behavior. Though being similar to M1−M3 data within 500 < T < 650 °C, it increases rapidly at T > 650 °C and at 750 °C it reaches ~0.23%/min (with an overall relative mass loss of 13%). Such a different dynamic may be attributed to the higher percentage of calcareous aggregates discussed in section 3 (see Table 3). According to [21] the concretes aggregated mostly with limestone show typical weight loss due to calcination of 20%–25% with DTG maximum located at around 900 °C.

4.2. Dielectric characterization

For the dielectric characterization cylindrical concrete samples (⌀ = 8 mm, h = 10 mm) were cut from the outer part of a bigger concrete specimen. After cutting, all samples were stored for more than 30 days in the same ambient, in-house atmosphere and temperature about 21 °C. Thus, before the experiment all samples are considered as air dried to equilibrium. Because the wavelength of the microwave is much larger than the characteristic scale of inhomogeneity (the mean size of aggregates concrete is about

1 cm) the dielectric properties of concrete at 2.45 GHz may be considered as effective or volume-averaged. Moreover, as the size of the concrete sample is of the same order as the size of the gravel aggregates a scatter in the dielectric properties of the concrete is expected depending on where the sample was cut from the concrete block. Therefore, to get a proper representation, three samples of each type of concrete have always been measured and results are averaged. In Fig. 4 the real and imaginary part of permittivity for all concretes under investigation are plotted versus temperature.

The temperature dependent dielectric measurements were performed with the following temperature cycle: RT → 700 °C → RT. This cycle is subdivided into two scenarios. In the first scenario the temperature is increased stepwise from room temperature to 700 °C. The stepwise heating implies that for every temperature step the sample was kept in the furnace for about 15 min and thereafter moved to the cavity for dielectric measurements (for about 3 s). The water diffusion coefficient of the concrete with w/c = 0.4 at room temperature is about $2 \cdot 10^{-8}$ m^2/s [22]. For the given size of sample this results in a characteristic time of moisture diffusion of about 13 min. At higher temperatures and for higher porosities (w/c > 0.4) this time is expected to be even shorter. Thus, both thermal and water concentration equilibriums are reached at every temperature step. For interval 25 … 200 °C the temperature steps were as high as 15 °C–25 °C, and for T > 200 °C they were 50 °C–100 °C.

First, we consider the behavior of permittivity measured during a heating scenario within three temperature intervals where three main reactions have been distinguished (same as for TG analysis), and thereafter during a cooling scenario.

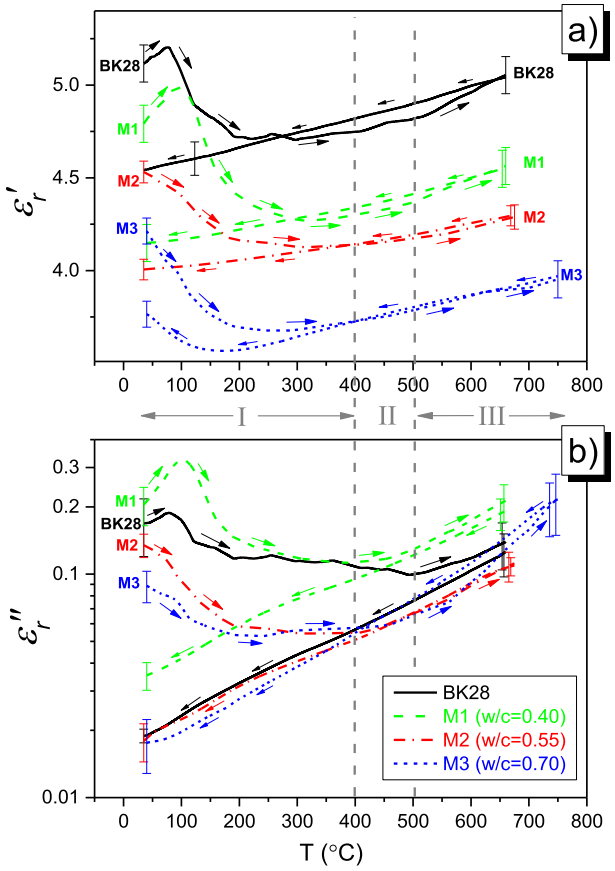

Fig. 4. Dielectric constant (a) and dielectric loss factor (b) for different grades of concrete measured during stepwise heating and during cooling scenarios. Labels I, II and III and grey vertical dashed lines indicate temperature regions. Arrows guide the development of permittivity along the temperature.

4.2.1. Permittivity in heating scenario from RT to 400 °C (region I)

At RT the measured real and imaginary part of permittivity for all concretes under investigation lie within 4.2 … 5.2 and 0.09 … 0.20, respectively. It agrees well with the data for dry concrete published in Refs. [10,13,14,16]. In the temperature range RT … 400 °C the changes in the effective permittivity of concrete is generally governed by the reactions of water which are overlapped with the increase of permittivity of solid constituents. Within RT … 100 °C temperature range the permittivity of concretes BK28 and M1 increases while permittivity of M2 and M3 grades decreases (this difference will be discussed in more detail in section 5.3) Above 100 °C the water evaporation is a dominating process and all four types of concrete reveal permittivity decrease which starts to be saturated at ~200 °C and thereafter reaches the minimum in the range from 250 °C to 300 °C. After the free water was evaporated from the concretes their minimal values are ranging as 3.7< ε_r' <4.7 and 0.05< ε_r'' <0.11.

4.2.2. Permittivity in heating scenario from 400 to 500 °C (region II)

In this temperature range the water, which is produced by thermal decomposition of calcium hydroxide, evaporates [21,23]. Because of this mass loss effect, some decrease in permittivity is expected. However, only $\varepsilon_r''(T)$ data for BK28 sample (which has for this reaction the most pronounced effect in TGA) show some decrease in region II. For all the rest $\varepsilon_r''(T)$ and $\varepsilon_r'(T)$ data the growing dynamic is not broken. Apparently the effect of water evaporation in M1–M3 grades (is indeed smaller than in BK28, see Fig. 3) is masked by the overall increase of permittivity in solid constituents.

4.2.3. Permittivity in heating scenario from 500 to 700 °C (region III)

In this temperature range the process of calcium carbonate decomposition (calcination) begins [21,23]. The composing aggregates such as a limestone and a sandstone with carbonate group dissociate into calcium oxide and carbon dioxide: $CaCO_3 \rightarrow CaO + CO_2\uparrow$. The product of this reaction, calcium oxide, is a stronger dielectric (ε_r' ~12) than calcium carbonate (ε_r' ~9). This effect together with a permittivity growth in solid constituents dominates the mass loss due to CO_2-release and results in a continuous increase of the effective permittivity of concrete.

4.2.4. Permittivity in cooling scenario

The cooling scenario starts several minutes after the end of the heating scenario from the highest temperature reached in the end of the heating scenario. During the cooling phase the sample is positioned permanently inside the cavity and cools back to the ambient temperature. In this scenario data are recorded with finer temperature steps: 1 °C–3 °C. The permittivities recorded during cooling phase are very different as compared with the data obtained in the heating scenario for the same temperatures (see Fig. 4). Because of the irreversible release of moisture and gas from the concrete, both ε_r' and ε_r'' within RT … 350 °C show significantly smaller values than those measured during the heating stage. Remarkably, within 350 … 700 °C range ε_r' in the cooling scenario somewhat exceeds the values measured during heating phase that can be a consequence of the irreversible transformation of $CaCO_3$ (ε_r' ~9) to CaO (ε_r' ~12) discussed in the section 4.2.3.

4.3. Penetration depth in the heating scenario

Based on the permittivity data obtained in heating scenario the microwave penetration depth for all four concrete grades in

measured temperature range is estimated. Penetration depth, d_p, is the distance from the surface where the microwave power is reduced by a factor of 1/e. We use here the approximation for plane waves [24]:

$$d_p = (1/2)\left[2\pi f\sqrt{\mu_0\varepsilon_0\varepsilon_r'/2}\ \sqrt{\sqrt{1+(\varepsilon_r''/\varepsilon_r')^2}-1}\right]^{-1}, \quad (1)$$

where f, μ_0 and ε_0 are the microwave frequency, permeability and permittivity of vacuum respectively. The results are presented in Fig. 5.

For denser concretes (BK28 and M1) and at $T < 300$ °C d_p varies within 15 … 35 cm whereas the penetration depth for lighter concretes (M2 and M3) lies within 30 … 70 cm. The penetration depth provides evidences on how localized the microwave power deposition is. For BK28 and M1 we can expect about 2 times higher absorbed power density as compared to M2 and M3. It is worthwhile to note, that unlikely to M2 and M3, penetration depth for BK28 and M1 grades decreases at the beginning of heating ($T \lesssim 100°C$). (This specific behavior of denser concretes will be discussed in detail in section 5.3). Such a behavior is beneficial because the absorbed power density in the surface layer increases with a decrease of d_p. Note, that for a real launcher when the incident wave diverges (not plane waves) the power deposition length is shorter than those in equation (1). This was confirmed by recent full-wave simulations for 2.45 GHz microwaves launched from antenna onto concrete block [25].

5. Discussion

5.1. Differences in water content for different concrete grades

The TG analysis (see Figs. 2 and 3) has shown that, the lower the w/c ratio, the higher is the water content in the concrete. It correlates well with the loss factor measurements (indeed $\varepsilon_r''_{water} \gg \varepsilon_r''_{solids}$) in the heating scenario: ε_r'' is the highest for M1 (w/c = 0.4), intermediate for M2 (w/c = 0.55) and the lowest for M3 (w/c = 0.7) grades (see Fig. 4b). At first glance it looks paradoxical, however for concrete layers close to the surface we should take into account the effects of water migration and evaporation. Water confined in the concrete is physically bound in pores which are different for cement paste and aggregates. For most aggregates, the relative pore volume is normally below 3% compared to 30 … 40% in the cement mortar [20]. (Note the porosity indicated in Table 1 is an average contribution of aggregates and cement paste). The mean pore size in aggregates is above 10 μm whereas the pore size of the cement paste is within 1 … 100 nm [20]. A consequence of a large pore size in aggregates is that at room temperature they are almost empty and most of concrete moisture is confined in the cement paste. Additionally, for the concrete dried to equilibrium (as in our case) most of capillaries in the cement mortar are also empty, but water in mesopores (3 … 30 nm) and micropores (<3 nm), so called strongly adsorbed water, is still there [26]. Thus, the higher representation of such pores in the concrete, the more water is confined. The analysis of pores distribution for M1–M3 concretes has shown that indeed the relative representation of pores with radii less than 30 nm is maximal for M1, intermediate for M2 and minimal for M3 [18].

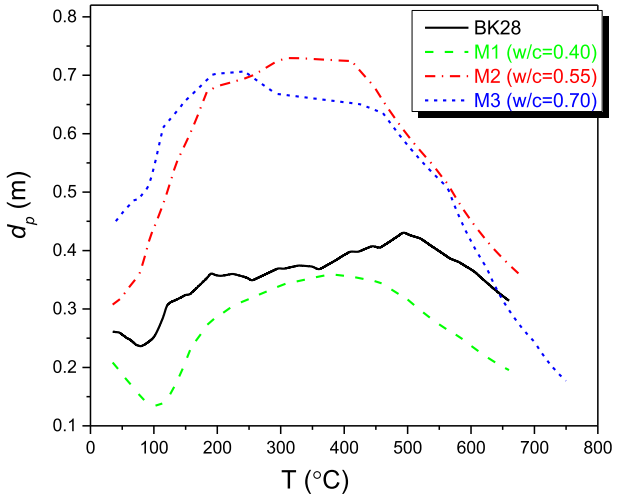

Fig. 5. Penetration depth for four grades of concrete during heating phase.

Because of much higher water content in the cement paste as compared to aggregates, most of the microwave energy will be absorbed in it resulting in high thermal gradients and vapor pressure in pores. Since thermal gradients and vapor pressure, are known to be the main factors defining the successful ablation of concrete [9], external (faced to atmosphere) layers of constructions made from the concretes with lower w/c ratio can be more effectively ablated than those made from concrete with higher w/c ratio.

5.2. Differences in permittivities at $T > 500$ °C

For temperatures above 500 °C the observed difference in the measured effective permittivity for different types of concrete cannot be attributed any more to the difference in moisture content, because all pores at this temperature are empty of water. Very likely, the differences in effective permittivity of concrete (more in ε' than in ε'') just follows the differences in the density of solid constituents, which to some extend are linked to differences in measured porosities indicated in Table 1. At the same time due to both dehydration and decarbonation processes the porosity of concrete increases non-linearly and at higher temperatures may be as high as 30%–50% [19]. Thus, the observed differences in the permittivity for $T > 500$ °C may be also referred to individual porosity behaviors.

Moreover, the lower siliceous and higher calcareous aggregation of BK28 concrete compared to lab-made concretes may explain its higher ε_r' and lower ε_r'' as compared to concrete M1 (concrete grade which is closest to BK28 with respect to porosity and temperature behavior). It correlates with results of Haddad et al. where the comparison of permittivities for Portland concrete cement aggregated with limestone was compared against one aggregated with quartzite [15].

5.3. Specific behavior of permittivity of denser concretes at $RT \lesssim T \lesssim 100°C$

It is a well-known effect when the viscosity of water molecules in the vicinity of hydrophobic surfaces increases. The loss of mobility of water molecules happens because of restriction in their orientation freedom. As a result the relaxation time of water bound in a concrete matrix (τ_{bw}) is increased as compared to free water (τ_w). The permittivity of water is a function of relaxation time and according to Debye equation for ensemble of dipolar molecules [27], reads

$$\varepsilon(\omega) = \varepsilon_w(\infty) + \frac{\varepsilon_w(0) - \varepsilon_w(\infty)}{1 + i\omega\tau}. \quad (2)$$

ω, ε_w (0) and ε_w (∞) are the angular frequency of the external field ($\omega = 2\pi f$), static permittivity ($\omega = 0$) of water and permittivity

of water at $\omega \to \infty$, respectively. The loss factor $\varepsilon'' = -\mathrm{Im}(\varepsilon)$ has a maximum at $\omega\tau = 1$. For bulk water at room temperature the relaxation time, τ_w is about 8 ps, and the ε''-maximum is at ~20 GHz [28]. In Fig. 6 the real and negative imaginary part of permittivity calculated in accordance with equation (2) for free ($\tau_w = 8$ ps) and bound ($\tau_{bw} = 200$ ps) water are plotted. The constants $\varepsilon_w(0)$ and $\varepsilon_w(\infty)$ for free and bound water are taken as 80.21 and 5.60 [28] and 57.90 and 3.15 [31], accordingly. For strongly bound water the relaxation time may be 1 to 3 orders of magnitude higher than for bulk water and the maximum in loss factor may be shifted significantly to the lower frequencies [28–30], even lower than 2.45 GHz (see Fig. 6).

Let us consider now the dynamics of permittivity of strongly bound water along increasing temperature. With the increase of temperature the relaxation time of water decreases thus resulting in a shift of gradient region of ε_r' and maximum of ε_r'' towards higher frequencies [27]. This shift is schematically shown in Fig. 6 with an arrow. Consequently, at a fixed frequency of 2.45 GHz both ε_r'' and ε_r' for strongly bound water are increasing with temperature. If this effect dominates water evaporation then the effective permittivity of concrete will grow up (and correspondingly d_p goes down). This apparently happens at the initial stage of heating (when the evaporation is not yet so intensive) for the case of M1 and BK28 grades of concrete (see the growth in ε_r' and ε_r'' at $T \lesssim 100°C$ in Fig. 4). In spite water evaporation at T>100 °C starts to dominate the $\varepsilon_r(T)$ dynamic, the competing effect described above still exists and may reduce the falling rate of $\varepsilon_r(T)$.

6. Conclusions

Dielectric characterization of dry concrete cured with different w/c ratios as well as of concrete cut from a nuclear power plant construction was performed at temperature cycle 25 °C → 700 °C → 25 °C. The measured dielectric constant and loss factor vary as $3.5 < \varepsilon_r' < 5.5$ and $0.05 < \varepsilon_r'' < 0.30$ depending on the temperature and heating history.

Since the amount of residual moisture in dry concrete is higher when the w/c ratio is lower, denser concretes M1 (w/c = 0.40) and BK28 (from reactor) being exposed to elevated temperature from 25 to 400 °C show two to three times higher dielectric loss factor as compared with lighter concretes prepared with w/c = 0.55 (M2) and 0.70 (M3). Accordingly, the microwave penetration depth for BK28 and M1 grades is about two times shorter than for M2 and M3 grades. It means that the concretes cured with lower w/c ratio (including the concrete from nuclear power plant) may be easier ablated/demolished/broken with microwaves than the concretes cured with the higher w/c ratio.

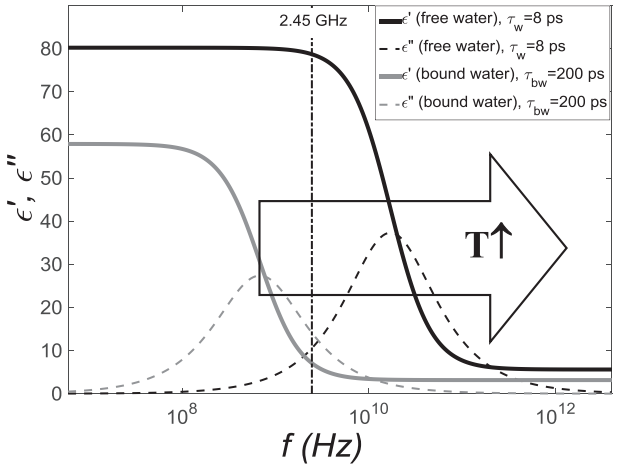

Fig. 6. Dielectric constant, ε', (solid) and loss factor, ε'', (dashed) according to Debye equation for free (τ = 8 ps) and bound (τ = 200 ps) water at room temperature. Operating frequency 2.45 GHz is shown with vertical dash-dotted line. Big arrow illustrates the shift of $\varepsilon'(f)$ and $\varepsilon''(f)$ dependencies towards higher frequencies with the temperature increase.

All concretes under investigation demonstrate almost similar dynamics of permittivity along increasing temperature. Their permittivities first decrease because of water evaporation, then get saturated at 300 < T < 400 °C, and thereafter increase due to the increase of permittivity of the solid constituents. Moreover, at the initial phase of heating ($T \lesssim 100°C$) the following peculiarity is found: the denser concretes, BK28 and M1, unlikely to lighter concretes M2 and M3, demonstrate the increase of permittivity with temperature. This effect — favorable for more effective and more localized microwave heating — was qualitatively explained in the framework of Debye model.

In the cooling scenario the permittivity of all concretes at T < 350 °C is found much lower as compared with the permittivity measured in the heating scenario at the same temperatures. The reason for that is the irreversible release of water and carbon dioxide from concretes at heating scenario.

Dielectric properties of the concrete taken from real nuclear power plant constructions (BK28) are mostly close to the concrete of grade M1 fabricated with w/c = 0.4. Note, the higher percentage of calcareous aggregates in BK28 as compared with lab-made M1–M3 grades.

We have investigated relatively small samples of ~0.5 cm^3 in a volume which were cut from bigger concrete blocks and dried to equilibrium for more than 30 days. Thus, the results presented are relevant to the outer layers of in-house, dry concretes influenced by environment atmosphere (moisture depletion, carbonation). The presented data may be useful for designing and modelling of applications such as microwave drying, microwave ablation and microwave drilling. However, with regards to repetitive ablation (layer by layer) the inner layers of concrete may have different permittivity.

Acknowledgments

The authors like to acknowledge Thomas Seitz and Stefan Layer for fabrication of experimental hardware. This research and development project is funded by the German Federal Ministry of Education and Research (BMBF) within the funding action “Decommissioning/Dismantling of Nuclear Facilities” (funding number 02S8719) and managed by the Project Management Agency Karlsruhe (PTKA).

References

[1] World Business Council for Sustainable Development, http://www.wbcsdcement.org/pdf/CSI-RecyclingConcrete-FullReport.pdf, (accessed 12.01.16).
[2] K.C. Gary Ong, Ali Akbarnezhad, Microwave-assisted Concrete Technology: Production, Demolition and Recycling, CRC Press, 2014.
[3] H.A. Püschner, Apparatus for Heating Material by Means of Microwave Device, United States Patent Office, May 6, 1969. Patent US 3443051, patented.
[4] S.C. Stone, Method for Fracturing Concrete and Other Materials with Microwave Energy, United States Patent Office, Aug. 1971. Patent US 3601448 A, patented 24.
[5] A. Watson, Methods of Cracking Structures and Apparatus for Cracking Structures, 1969. US Patent 3430021, issued February 25.
[6] T.L. White, R.G. Grubb, L.P. Pugh, D. Foster, W.D. Box, Removal of contaminated concrete surfaces by microwave heating – phase I results, in: Proceedings of the 18th American Nuclear Society Symposium on Waste Management, Tuscon, Arizona, March 1992.
[7] T.L. White, D. Foster, C.T. Wilson, C.R. Schaich, Phase II Microwave Concrete Decontamination Results, ORNL Rep. No. DE-AC05–84OR21400, National Laboratory, Oak Ridge, TN, 1995.

[8] P.J.M. Monteiro, A.P. Kirchheim, S. Chae, P. Fischer, A.A. MacDowell, E. Schaible, et al., Characterizing the nano and micro structure of concrete to improve its durability, Cem. Concr. Compos. 31 (2009) 577–584.
[9] Z.P. Bažant, F. Asce, G. Zi, Decontamination of radionuclides from concrete by microwave heating. I: theory, J. Eng. Mech. (2003) 777.
[10] W. Li, M.A. Ebadian, T.L. White, R.G. Grubb, D. Foster, Heat and mass transfer in a contaminated porous concrete slab with variable dielectric properties, Int. J. Heat. Mass Transf. 37 (6) (April 1994) 1013–1027.
[11] A. Akbarnezhad, K.C.G. Ong, M.H. Zhang, C.T. Tam, T.W.J. Foo, Microwave-assisted beneficiation of recycled concrete aggregates, Constr. Build. Mater. 25 (2011) 3469–3479.
[12] K.C.G. Ong and A. Akbarnezhad, Thermal stresses in the microwave heating of concrete, Proceeding of 31st Conf. on Our World in Concrete & Structures, 16–17 August 2006, Singapore, http://cipremier.com/100031038, (accessed 12.01.16).
[13] H.C. Rhim, O. Büyüköztürk, Electromagnetic properties of concrete at microwave frequency range, ACI Mater. J. 95 (No. 3) (May-June 1998) 262–271.
[14] M.N. Soutsos, J.H. Bungey, S.G. Millard, M.R. Shaw, A. Patterson, Dielectric properties of concrete and their influence on radar testing, NDT E Int. 34 (Issue 6) (September 2001) 419–425.
[15] R.H. Haddad, I.L. Al-Qadi, Characterization of Portland cement concrete using electromagnetic waves over the microwave frequencies, Cem. Concr. Res, 28 (10) (October 1998) 1379–1391, http://dx.doi.org/10.1016/S0008-8846(98)00076-3. ISSN 0008-8846.
[16] O. Büyüköztürk, T.-Y. Yu, J.A. Ortega, A methodology for determining complex permittivity of construction materials based on transmission-only coherent, wide-bandwidth free-space measurements, Cem. Concr. Compos. 28 (2006) 349–359.
[17] S. Soldatov, T. Kayser, G. Link, J. Jelonnek, Microwave cavity perturbation technique for high-temperature dielectric measurements, in: Proceedings of the IEEE MTT-S International Microwave Symposium 2013, Seattle, USA, June 2013, http://dx.doi.org/10.1109/MWSYM.2013.6697793.
[18] H.S. Müller, M. Umminger, M. Haist, G. Link, B. Lepers, Ablation Kontaminierter Oberflächen Zementgebundener Bauteile Beim Rückbau Kerntechnischer Anlagen, Final Report German Federal Ministry of Education and Research (BMBF) research projects 02S8709 and 02S8719, Karlsruhe Institute of Technology, 2015.
[19] D.J. Naus, A Compilation of Elevated Temperature Concrete Material Property Data and Information for Use in Assessments of Nuclear Power Plant Reinforced Concrete Structures, NUREG/CR-7031 ORNL/TM-2009/175, Nuclear Regulatory Commission, U.S, 2010.
[20] P. Mehta, P.J.M. Monteiro, Concrete: Microstructure, Properties, and Materials, The McGraw-Hill Companies Inc, 2006.
[21] G. Villain, M. Thiery, G. Platret, Measurement of carbonation profiles in concrete: thermogravimetry, chemical analysis and gammadensimetry, Cem. Concr. Res. 37 (2007) 1182–1192.
[22] B. Pradhan, M. Nagesh, B. Bhattacharjee, Prediction of the hydraulic diffusivity from pore size distribution of concrete, Cem. Concr. Res. 35 (2005) 1724–1733.
[23] D.R. Flynn, Response of High Performance Concrete to Fire Conditions: Review of Thermal Property Data and Measurement Techniques, NIST GCR 99–767, Report prepared for U.S, Department of Commerce Building and Fire Research Laboratory NIST, 1999.
[24] A.C. Metaxas, Foundations of Electroheat, John Wiley & Sons, 1996.
[25] B. Lepers, A. Putranto, M. Umminger, G. Link, J. Jelonnek, A drying and thermoelastic model for fast microwave heating of concrete, Front. Heat Mass Transf. (FHMT) 5 (2014) 13.
[26] H.M. Jennings, Colloid model of C-S-H and implications to the problem of creep and shrinkage, materials and structures, Special Issue Concr. Sci. Eng. Poromechanics Cement-Based Mater. 37 (265) (2004) 59–70.
[27] P. Debye, Polar Molecules, Dover Publications, Inc., New York, 1929.
[28] U. Kaatze, Complex permittivity of water as a function of frequency and temperature, J. Chem. Eng. Data 34 (1989) 371–374.
[29] C. Colosi, M. Costantini, A. Barbetta, C. Cametti, M. Dentini, Anomalous Debye-like dielectric relaxation of water in micro-sized confined polymeric systems, Phys.Chem. Chem. Phys. 15 (2013) 20153.
[30] S. Mashimo, S. Kuwabara, S. Yagihara, K. Higasi, Dielectric relaxation time and structure of bound water in biological materials, J. Phys. Chem. 91 (1987) 6337–6338.
[31] J. Behari, Microwave Dielectric Behaviour of Wet Soils, Springer, New Delhi, India, 2005.